DOI: 10.1002/anie.201101536

Drug Delivery

pH-Tunable Calcium Phosphate Covered Mesoporous Silica Nanocontainers for Intracellular Controlled Release of Guest Drugs**

Hwa Pyeong Rim, Kyung Hyun Min, Hong Jae Lee, Seo Young Jeong, and Sang Cheon Lee**

Mesoporous silica nanoparticles (Si-MPs) have emerged as appealing hosts for the exploitation of novel nanocarriers featuring "on demand" drug delivery.[1–3] To date, a variety of stimuli-responsive "pore blockers", such as organic molecules (cyclodextrin, dendrimer),[4,5] metal (gold) nanoparticles,[6] and supramolecular assemblies (rotaxanes, polyrotaxanes),[7,8] have been introduced on the surfaces of Si-MPs to control the release of guest molecules in response to external stimuli. Various physical/chemical stimuli, such as pH,[8–10] photoirradiation,[4,6] redox potential,[11] and enzymes,[12–14] have been used as triggers for uncapping the pore blockers and releasing encapsulated guest molecules. Although these Si-MPs hold promise as potential delivery vehicles, many of the pore-blocking species have critical drawbacks for clinical applications because dismantled pore-blocking agents, for which body toxicity has not been well defined, can induce toxic side effects. Therefore, the design of Si-MP nanocarriers that use a natural nontoxic component as pore blocker remains a significant challenge. Very recently, Si-MPs with nucleic acids[15] and carbohydrates[16] as molecular valves have been reported for controlled-release devices, and recognized as valuable trials of using organic biomolecules as pore-blocking species. This effort toward the introduction of natural components may offer useful guidance to the practical use of Si-MPs for in vivo biological applications.

Herein, we report a novel Si-MP carrier covered with pH-controlled, absorbable calcium phosphate (CaP) nanocoatings as pore blockers that allow the facilitated release of entrapped drugs within acidifying intracellular compartments such as endosomes and lysosomes. Our major aim is to develop a new, natural pore blocker, especially one based on nontoxic inorganic biominerals. CaP is the main component in bone and plays a key role in the natural bone regeneration process.[17,18] CaP is widely used as a bioactive osteoconductive coating for bone-regenerative materials, and these coating processes currently rely on time-consuming procedures in simulated body fluid (SBF) for several weeks.[19] Our research has recently centered on a unique feature of CaP; it can be dissolved as nontoxic ions (calcium, phosphate ions) in acidic cellular environments such as endosomes (pH ca. 5.0) and lysosomes (pH ca. 4.5).[20,21] In a previous report, we demonstrated the feasibility of pH-controlled release of doxorubicin (DOX), an anticancer drug, from mineralized polymer nanoparticles in the endo/lysosomes of breast cancer MCF-7 cells.[21]

The key idea is urease functionalization of Si-MP surfaces and subsequent enzyme-mediated surface CaP mineralization in the presence of urea under mild conditions for a short time period. Figure 1a and c illustrate the overall process for surface anchoring of urease, the subsequent CaP coating of Si-MP surfaces, and controlled release of DOX within cells. For this purpose, we prepared Si-MP-0 with a mean diameter of 100 nm (Figure 1b), an average pore diameter of 2.5 nm (Barret–Joyner–Halenda (BJH) analysis), and a specific surface area of $900.5\ m^2g^{-1}$ (Brunauer–Emmett–Teller (BET) analysis). The surface of Si-MP-0 was functionalized with primary amine groups by the reaction of 3-aminopropyltriethoxysilane (APTES) to provide Si-MP-NH_2, which was further allowed to react with glutaraldehyde to obtain Si-MP-COH. Primary amines and aldehydes of Si-MP-NH_2 and Si-MP-COH exhibited an N–H bending vibration at $1580\ cm^{-1}$ and C=O stretching at $1645\ cm^{-1}$ (Figure S1 in the Supporting Information). To prepare urease-functionalized Si-MPs (Si-MP-UR), urease was covalently conjugated through reaction with surface aldehydes (Schiff's base formation).

Transmission electron microscopy (TEM) and powder X-ray diffraction (XRD) analyses revealed that Si-MP-UR exhibits a well-ordered porous structure with a hexagonal arrangement (Figure 2a and c, and Figure S1b in the Supporting Information). For CaP nanocoatings, Si-MP-UR was placed in a mineralizing acidic solution (pH 4.0) containing hydroxyapatite (HAp, $Ca_5(PO_4)_3OH$) and urea. It is known that surface-conjugated urease catalyzes urea hydrolysis into ammonium bicarbonate and hydroxide ions in a pH range of 4.0–9.5: $OC(NH_2)_2 + 2H_2O \rightarrow 2NH_4^+ + HCO_3^- + OH^-$.[22,23] It is well known that the surface silanols of silica present a negative charge at neutral pH, which can lead to the formation of an electric double layer with calcium cations.[22] The presence of PO_4^{3-} and released OH^- ions by urea decomposition increased the ionic concentration above the

[*] H. P. Rim,[+] K. H. Min,[+] Prof. Dr. S. Y. Jeong
Department of Life and Nanopharmaceutical Science
Kyung Hee University
1 Hoegi-dong, Dongdaemun-gu, Seoul 130-701 (Korea)
E-mail: syjeong@khu.ac.kr
H. J. Lee, Prof. Dr. S. C. Lee
Department of Maxillofacial Biomedical Engineering &
Institute of Oral Biology, School of Dentistry
Kyung Hee University
1 Hoegi-dong, Dongdaemun-gu, Seoul 130-701 (Korea)
E-mail: schlee@khu.ac.kr
[+] These authors contributed equally to this work.

[**] This research was supported by a grant (code: 2011K000186) from the Center for Nanostructured Materials Technology under the "21st Century Frontier R&D Programs" of the Ministry of Education, Science, and Technology, Korea.

Supporting information for this article is available on the WWW under http://dx.doi.org/10.1002/anie.201101536.

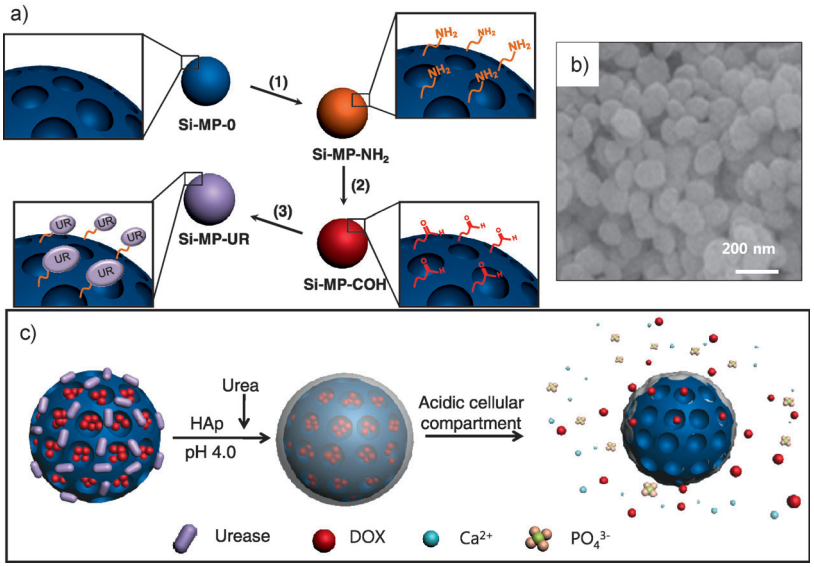

Figure 1. a) Synthetic route to Si-MP-UR: 1) APTES; 2) removal of cetyltrimethylammonium bromide, glutaraldehyde; 3) Jack bean urease (UR). b) Field-emission scanning electron microscopy image of Si-MP-UR. c) Schematic of surface CaP mineralization of DOX-loaded Si-MP-UR and triggered drug release under intracellular endo/lysosomal conditions. HAp = hydroxyapatite.

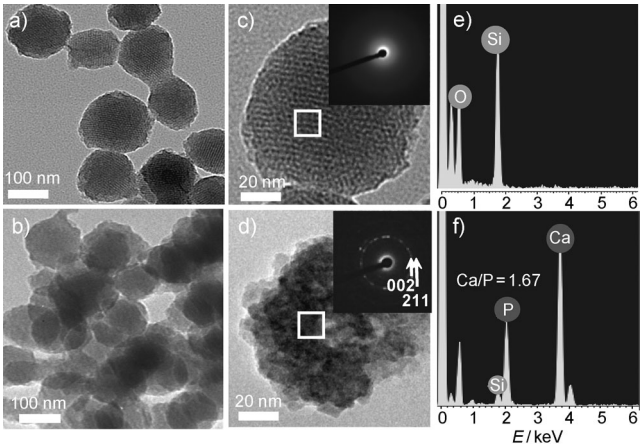

Figure 2. TEM images of a) Si-MP-UR and b) DOX-Si-MP-CaP. Enlarged TEM images and SAED patterns of indicated areas for c) Si-MP-UR and d) DOX-Si-MP-CaP. TEM-associated EDX spectra e) before and f) after the mineral coating.

critical saturation point to trigger the deposition of CaP minerals on silica surfaces. In response to the increased pH (ca. 9), it is expected that Ca^{2+} and PO_4^{3-} ions (ionic sources from HAp dissolution at pH 4.0) are precipitated with OH^- ions to form HAp-like coatings on the surface of Si-MP-UR, depending on the following stoichiometric equation: $5Ca^{2+} + 3PO_4^{3-} + OH^- \rightarrow Ca_5(PO_4)_3OH$. As illustrated in Figure 1c, DOX guest molecules were loaded into the pores by soaking Si-MP-UR in a DOX solution. DOX-loaded Si-MP-UR was added to an acidic solution of HAp and urea (pH 4.0) to produce DOX-loaded Si-MP-CaP, in which the pores were capped by CaP coatings through the urease-mediated surface mineralization. The excess DOX and urea were removed by filtration, centrifugation, and washing with distilled water (pH 7.4).

Figure 2 shows the surface morphological/elemental change of Si-MP-UR after mineralization. The initially smooth surface of Si-MP-UR generated rough coatings featuring a flakelike assembly (Figure 2b and d). It is noteworthy that the open mesopore structure of Si-MP-UR (Figure 2c) could not be identified, which indicates mesopore blocking during the mineralization process (Figure 2d). TEM-associated selected-area electron diffraction (SAED) analysis showed the change in the diffraction pattern after mineralization. The diffraction pattern of the surfaces of mineralized DOX-Si-MP-CaP showed *d* spacings corresponding to that of HAp (lattice parameters of $a = 9.422$ and $c = 6.883$ Å; Figure 2d).[24] In addition, TEM-associated energy-dispersive X-ray spectroscopy (EDX) analysis showed that mineralized surfaces predominantly contained Ca and P, which belong to CaP minerals (Figure 2f). The Ca/P molar ratio was estimated as about 1.67, which indicates that the major phase of mineral coatings is HAp.[25] Therefore, it is confirmed that the surface mineralization process induced the nucleation and growth of HAp-like nanocoatings on mesoporous particle surfaces.

Wide-angle XRD patterns also showed that DOX-Si-MP-CaP exhibited the characteristic sharp peaks of HAp, (211), (300), and (202), although a small portion of broad peak areas for premature amorphous CaP was found (Figure S2 in the Supporting Information). The N_2 adsorption–desorption studies showed that DOX-Si-MP-UR has the greatly reduced surface area of 151.3 $m^2 g^{-1}$, caused by the pore-filling effect of DOX. Interestingly, DOX-Si-MP-CaP exhibited the further decreased surface area of 23.9 $m^2 g^{-1}$ and pore size distribution (Table S1 and Figure S3 in the Supporting Information). This indicates the pore-blocking effect of the HAp coatings after surface mineralization. Zeta potential measurement showed that the mineralized DOX-Si-MP-CaP nanoparticles had a slightly negative value ($\zeta = -2.6$ mV), which was similar to the value previously reported for the HAp nanoparticles (Figure S4 in the Supporting Information).[21,26] Using dynamic light scattering, the stability of DOX-Si-MP-CaP in phosphate-buffered saline (PBS, pH 7.4, 10 mM) solution and serum solution (50% fetal bovine serum) was estimated. DOX-Si-MP-CaP maintained the nanoparticle stability in both the PBS and serum solutions, as judged by the constant mean diameter and scattered light intensities (Figure S5 in the Supporting Information).

To verify that surface-conjugated urease is a major factor for surface HAp-like mineral coatings, the free urease was incubated with Si-MP-0, urea, and HAp at pH 4.0, as a control experiment. It is noteworthy that the Si-MP surface was not coated by HAp minerals, and needlelike HAp crystals were separately formed through homogeneous solution precipitation (see the TEM image and EDX data in Figure S6 in the

Supporting Information). Thus, we reached the solid conclusion that the surface immobilization of urease resulted in the successful coating of the Si-MP surface through surface heterogeneous nucleation and growth of minerals.

It is known that the aqueous solubility of HAp is dependent on pH and dramatically increases below about pH 5.0, whereas it can maintain the solid mineral structure at physiological pH.[27] In particular, HAp is known as the most thermodynamically stable CaP phase in the physiological environment.[28] Therefore, it is expected that the HAp-like pore-blocking coating can prevent premature release of the encapsulated drug from mesopores at unwanted extracellular compartments. In addition, HAp-like coatings can be dissolved at the endosome/lysosome of target disease cells to trigger encapsulated drug molecules.

For pH-controlled DOX release from mineralized Si-MPs, we employed pH variation between physiological pH (pH 7.4) and the low pH condition (pH 4.5). DOX was loaded into Si-MPs at 4.2 wt% by a diffusion method. The DOX loading in Si-MP-CaP was visualized by confocal laser scanning microscopy (Figure S7 in the Supporting Information). Figure 3a shows the DOX release profiles from nonmineralized DOX-Si-MP-UR and mineralized DOX-Si-MP-CaP at physiological pH values and the low pH condition. DOX-Si-MP-UR showed a fast DOX release rate irrespective of the pH value of the release medium. DOX-Si-MP-UR has open pores and lacks the pore-blocking species; thus it could not prevent DOX release at physiological pH values. Following a negligible initial release, probably stemming from surface-bound DOX, DOX-Si-MP-CaP did not show any release at physiological pH values. On the other hand, facilitated DOX release was triggered under the low pH condition. DOX-Si-MP-CaP released a large amount of DOX (81.4%) even after 1 day.

To support the release profiles of DOX from DOX-Si-MP-CaP, the pH-dependent dissolution kinetics of HAp-like coatings from DOX-Si-MP-CaP were investigated. As shown in Figure 3c, the mineral coating underwent minimal initial dissolution (<5%) under the physiological pH condition, which can be expected from the premature amorphous CaP of high water solubility. However, after 1 h the coating of HAp-like pore blockers was maintained. In contrast, under the low pH condition, accelerated dissolution of HAp-like coatings was found. This is understood in that the solubility of HAp increases in proportion to the concentration of protons.[27] Dissolution of pore blockers results in the opening of the pore, thereby triggering DOX release.

The in vitro cytotoxicity of DOX-Si-MP-UR and DOX-Si-MP-CaP was examined with breast cancer MCF-7 cells. For concentrations up to 250 μg mL^{-1}, Si-MP-UR and mineralized Si-MP-CaP were not cytotoxic (Figure S8 in the Supporting Information). As shown in Figure 4 and Table 1, DOX-Si-MP-CaP showed relatively low toxicity in comparison to free DOX and DOX-Si-MP-UR. The somewhat lower toxicity of DOX-Si-MP-CaP, compared to free DOX and DOX-Si-MP-UR, was probably due to the gradual release of DOX within the cells and different cellular localization of the drugs. Nonmineralized DOX-Si-MP-UR immediately began releasing DOX upon placement in the cell culture medium. In contrast, the DOX release rate from DOX-Si-MP-CaP was slower, because the release was accelerated after dissolution of the mineral coating within cellular lysosomes. The potential not only for minimizing drug loss in blood but also for selective accumulation in tumor tissue by the enhanced permeation and retention (EPR) effect may enhance its overall therapeutic efficacy in vivo relative to free DOX and DOX-loaded nonmineralized Si-MPs.

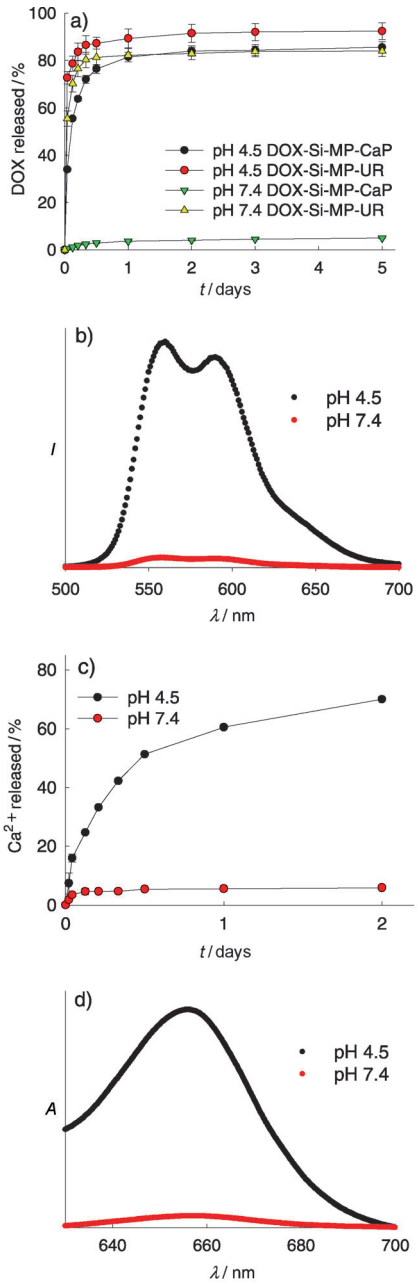

Figure 3. a) DOX release profiles from DOX-Si-MP-UR and DOX-Si-MP-CaP under pH control. b) Fluorescence spectra of DOX (λ_{ex} = 480 nm) after 5 h of incubation of DOX-Si-MP-CaP at different pH values. c) Kinetics of calcium dissolution from DOX-Si-MP-CaP under pH control. d) Absorption spectra of Arsenazo III/Ca^{2+} complex after 5 h of incubation of DOX-Si-MP-CaP at different pH values.

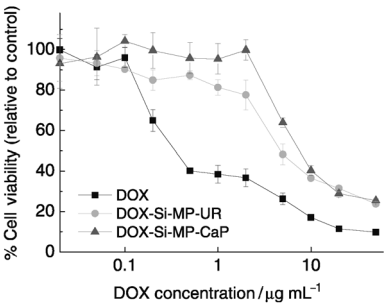

Figure 4. In vitro cytotoxicity of DOX, DOX-Si-MP-UR, and DOX-Si-MP-CaP with MCF-7 cells after 24 h ($n=3$).

Table 1: IC_{50} values of DOX and DOX-loaded nanoparticles.

Sample	$IC_{50} \pm SD$ [$\mu g\,mL^{-1}$][a]
free DOX	0.34 ± 0.03
DOX-Si-MP-UR	4.58 ± 0.7*
DOX-Si-MP-CaP	7.54 ± 0.48*

[a] Mean IC_{50} value $\pm$ standard deviation (SD; $n=3$). *$P<0.01$ relative to free DOX.

The endocytosis of DOX-Si-MP-CaP containers by MCF-7 cells was monitored by confocal laser scanning microscopy (CLSM). The acidic cellular compartment was labeled with green-fluorescent LysoTracker as an indicator. After 1 h of incubation, MCF-7 cells treated with DOX-Si-MP-CaP exhibited a bright red fluorescence within the acidic cytoplasm, but a negligible DOX fluorescence within nuclei (Figure 5b). After a further 4 h of incubation, a strong fluorescence was found in nuclei, which can be ascribed to the released DOX from internalized DOX-Si-MP-CaP. DOX not only spread out in lysosomes but also accumulated in the nuclei (Figure 5c). This suggests that a triggering factor for DOX release was the dissolution of mineral coatings in acidic cellular compartments. On the other hand, DOX-Si-MP-UR showed stronger red fluorescence within nuclei than DOX-Si-MP-CaP (Figure 5d) even after 1 h of incubation. This indicates that DOX-Si-MP-UR began to release DOX upon addition to the cell culture medium. In other words, DOX-Si-MP-UR tended to induce fast DOX release in the extracellular area, and the released DOX was localized within nuclei in a short time period. This finding is consistent with the DOX release patterns from DOX-Si-MP-UR at pH 7.4 (Figure 3a). Based on in vitro results, we confirmed that the HAp-like pore-blocking coating of DOX-Si-MP-CaP is effective in holding DOX before endocytosis, and the DOX release can be facilitated within lysosomes by the dissolution of HAp-like coatings.

We next evaluated the in vivo efficacy of DOX-Si-MP-CaP using xenograft models of MCF-7 human breast cancers. Figure 6 shows that a single intratumoral administration of DOX-Si-MP-CaP is significantly more efficacious in tumor reduction than control groups including free DOX and DOX-Si-MP-UR.

One reason for the enhanced in vivo efficacy might be the delayed clearance of DOX-Si-MP-CaP at the tumor site because of the retention property of the nanoparticles.[29] In addition, the protection of pore-blocked DOX against rapid clearance before endocytosis and the subsequent intracellular release of DOX may contribute to the enhanced antitumor effect. The treatments with free DOX or DOX-Si-MP-UR were also effective in tumor regression to some extent, but did not show a comparable efficacy to DOX-Si-MP-CaP, possibly as a result of the small size of free DOX or extracellularly released DOX that would be rapidly diffused away from the tumor interstitium.[29]

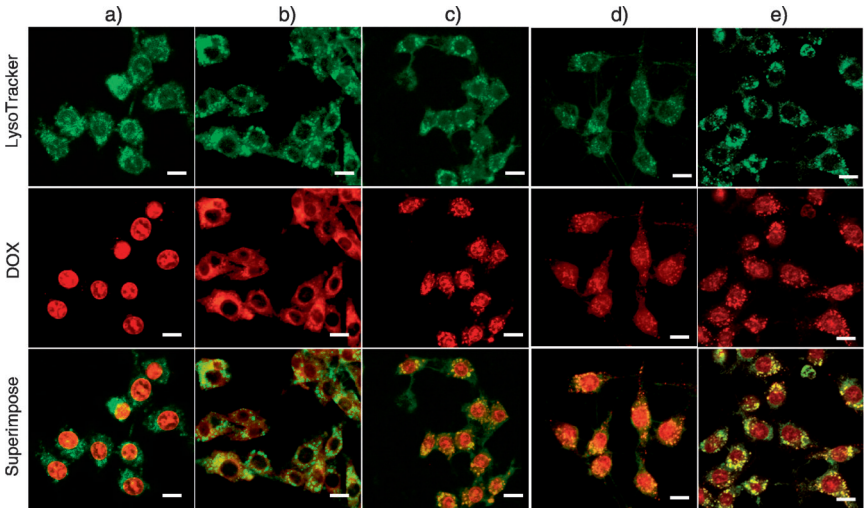

Figure 5. CLSM images of live MCF-7 cells treated with LysoTracker (50 nM), free DOX (5 $\mu g\,mL^{-1}$), and DOX-Si-MP-CaP (DOX = 5 $\mu g\,mL^{-1}$). a) Free DOX for 1 h exposure, b) DOX-Si-MP-CaP for 1 h exposure, c) DOX-Si-MP-CaP for 5 h exposure, d) DOX-Si-MP-UR for 1 h exposure, and e) DOX-Si-MP-UR for 5 h exposure. (Green fluorescence is associated with LysoTracker; the red fluorescence is expressed by free DOX, released DOX, and DOX retained within Si-MPs.) Scale bar: 20 μm.

In summary, we have demonstrated that the introduction of inorganic CaP as a novel pore blocker by enzyme-mediated mineralization on the Si-MP surfaces provides a novel route for smart porous nanocarriers, which are capable of releasing guest drugs from the CaP-blocked pore under pH control. The CaP coatings can hold the encapsulated anticancer drugs under extracellular conditions, whereas they can be dissolved within intracellular endosomes as nontoxic ions to initiate drug release within tumor cells. The in vivo efficacy of DOX-loaded Si-MP-CaP was confirmed using xenograft models of MCF-7 human breast cancers. Mineral-coated Si-MPs may satisfy the major requirements for cancer chemotherapy with a high delivery efficiency: 1) high structural stability in blood, 2) minimized premature drug release, and 3) release of drugs specifically within tumor cells. The Si-MPs covered with biocompatible CaP coat-

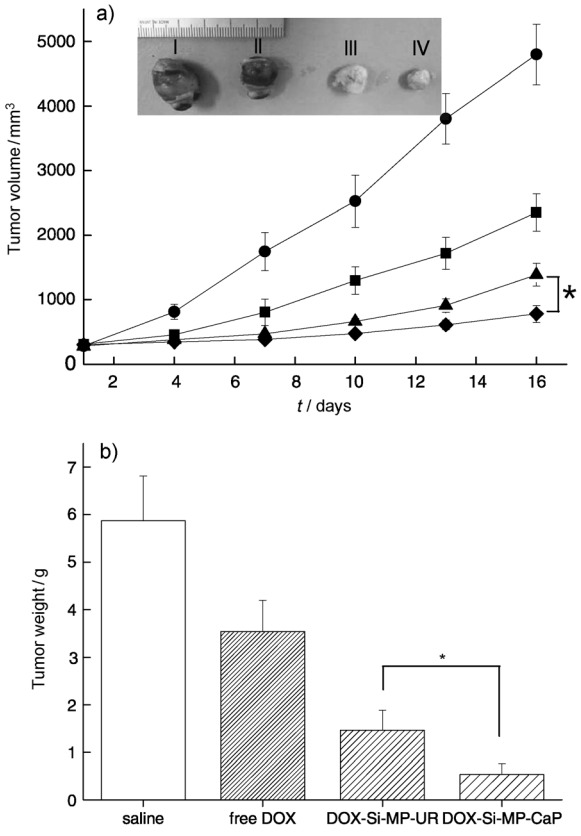

Figure 6. a) In vivo therapeutic efficacy after a single intratumoral injection of saline (●), free DOX (■), DOX-Si-MP-UR (▲), and DOX-Si-MP-CaP (◆) at a DOX-equivalent dose of 10 mg kg^{-1}. Inset: images of excised tumors after 16 days post-treatment. I: saline, II: free DOX, III: DOX-Si-MP-UR, IV: DOX-Si-MP-CaP. b) Tumor weights after 16 days post-treatment. The results represent the means ± SDs ($n = 4$); $^*P < 0.05$.

ings might serve as promising specific intracellular carriers for many drugs, proteins, and imaging agents.

Received: March 2, 2011
Revised: May 31, 2011
Published online: August 8, 2011

Keywords: drug delivery · host–guest systems · mesoporous materials · mineralization · nanoparticles

[1] H. Kim, S. Kim, C. Park, H. Lee, H. J. Park, C. Kim, *Adv. Mater.* **2010**, *22*, 4280 – 4283.
[2] Y. Zhao, B. G. Trewyn, I. I. Slowing, V. S.-Y. Lin, *J. Am. Chem. Soc.* **2009**, *131*, 8398 – 8400.
[3] H. S. Park, C. W. Kim, H. J. Lee, J. H. Choi, S. G. Lee, Y.-P. Yun, I. C. Kwon, S. J. Lee, S. Y. Jeong, S. C. Lee, *Nanotechnology* **2010**, *21*, 225101.
[4] C. Park, K. Lee, C. Kim, *Angew. Chem.* **2009**, *121*, 1301 – 1304; *Angew. Chem. Int. Ed.* **2009**, *48*, 1275 – 1278.
[5] D. R. Radu, C.-Y. Lai, K. Jeftinija, E. W. Rowe, S. Jeftinija, V. S.-Y. Lin, *J. Am. Chem. Soc.* **2004**, *126*, 13216 – 13217.
[6] J. L. Vivero-Escoto, I. I. Slowing, C.-W. Wu, V. S.-Y. Lin, *J. Am. Chem. Soc.* **2009**, *131*, 3462 – 3463.
[7] T. D. Nguyen, Y. Liu, S. Saha, K. C.-F. Leung, J. F. Stoddart, J. I. Zink, *J. Am. Chem. Soc.* **2004**, *129*, 626 – 634.
[8] C. Park, K. Oh, S. C. Lee, C. Kim, *Angew. Chem.* **2007**, *119*, 1477 – 1479; *Angew. Chem. Int. Ed.* **2007**, *46*, 1455 – 1457.
[9] H. Meng, M. Xue, T. Xia, Y.-L. Zhao, F. Tamanoi, J. F. Stoddart, J. I. Zink, A. E. Nel, *J. Am. Chem. Soc.* **2010**, *132*, 12690 – 12697.
[10] Y.-L. Zhao, Z. Li, S. Kabehie, Y. Y. Botros, J. F. Stoddart, J. I. Zink, *J. Am. Chem. Soc.* **2010**, *132*, 13016 – 13025.
[11] R. Lui, X. Zhao, T. Wu, P. Feng, *J. Am. Chem. Soc.* **2008**, *130*, 14418 – 14419.
[12] C. Park, H. Kim, S. Kim, C. Kim, *J. Am. Chem. Soc.* **2009**, *131*, 16614 – 16615.
[13] K. Patel, S. Angelos, W. R. Dichtel, A. Coskun, Y.-W. Yang, J. I. Zink, J. F. Stoddart, *J. Am. Chem. Soc.* **2008**, *130*, 2382 – 2383.
[14] A. Schlossbauer, J. Kecht, T. Bein, *Angew. Chem.* **2009**, *121*, 3138 – 3141; *Angew. Chem. Int. Ed.* **2009**, *48*, 3092 – 3095.
[15] A. Schlossbauer, S. Warncke, P. M. E. Gramlich, J. Kecht, A. Manetto, T. Carell, T. Bein, *Angew. Chem.* **2010**, *122*, 4842 – 4845; *Angew. Chem. Int. Ed.* **2010**, *49*, 4734 – 4737.
[16] A. Bernardos, E. Aznar, M. D. Marcos, R. Martínez-Máñez, F. Sancenón, J. Soto, J. M. Barat, P. Amorós, *Angew. Chem.* **2009**, *121*, 5998 – 6001; *Angew. Chem. Int. Ed.* **2009**, *48*, 5884 – 5887.
[17] L. Zhao, M. D. Weir, H. H. K. Xu, *Biomaterials* **2010**, *31*, 6502 – 6510.
[18] S. E. Kim, H. W. Choi, H. J. Lee, J. H. Chang, J. Choi, K. J. Kim, H. J. Lim, Y. J. Jun, S. C. Lee, *J. Mater. Chem.* **2008**, *18*, 4994 – 5001.
[19] X. Liu, L. A. Smith, J. Hu, P. X. Ma, *Biomaterials* **2009**, *30*, 2252 – 2258.
[20] Q. Yang, S. Wang, P. Fan, L. Wang, Y. Di, K. Lin, F.-S. Xiao, *Chem. Mater.* **2005**, *17*, 5999 – 6003.
[21] H. J. Lee, S. E. Kim, I. K. Kwon, C. Park, C. Kim, J. Yang, S. C. Lee, *Chem. Commun.* **2010**, *46*, 377 – 379.
[22] I. Ortega, M. Jobbágy, M. L. Ferrer, F. del Monte, *Chem. Mater.* **2008**, *20*, 7368 – 7370.
[23] J. V. de Melo, S. Cosnier, C. Mousty, C. Martelet, N. Jaffrezic-Renault, *Anal. Chem.* **2002**, *74*, 4037 – 4043.
[24] H. J. Lee, H. W. Choi, K. J. Kim, S. C. Lee, *Chem. Mater.* **2006**, *18*, 5111 – 5118.
[25] A. Phadke, C. Zhang, Y. S. Hwang, K. Vecchio, S. Varghese, *Biomacromolecules* **2010**, *11*, 2060 – 2068.
[26] S. C. Lee, H. W. Choi, H. J. Lee, K. J. Kim, J. H. Chang, S. Y. Kim, J. Choi, K.-S. Oh, Y.-K. Jeong, *J. Mater. Chem.* **2007**, *17*, 174 – 180.
[27] H.-B. Pan, B. W. Darvell, *Cryst. Growth Des.* **2009**, *9*, 639 – 645.
[28] S. Koutsopoulos, *Langmuir* **2001**, *17*, 8092 – 8097.
[29] K. J. Harrington, G. Rowlinson-Busza, K. N. Syrigos, P. S. Uster, R. G. Vile, J. S. W. Stewart, *Clin. Cancer Res.* **2000**, *6*, 2528 – 2537.

